Emergence and Visualization of an Interface State during Contact Formation with a Single Molecule

P. M. Ryan,[1] L. C. Teague,[1,*] B. Naydenov,[1] D. Borland,[2] and John J. Boland[1]

[1]School of Chemistry and Center for Research on Adaptive Nanostructures and Nanodevices (CRANN), Trinity College Dublin, Dublin 2, Ireland

[2]RENCI at University of North Carolina Chapel Hill, Chapel Hill, North Carolina, USA

(Received 31 March 2008; published 25 August 2008)

Contact formation dynamics and electronic perturbations arising from the interaction of a metallic probe and a single molecule (1,3 cyclohexadiene) bound on the Si (100) surface are examined using a series of plane wave, density functional theory calculations. The approach of the probe induces a relaxation of the molecule that ultimately leads to the formation of an interface state due to a specific interaction between the probe apex atom and the C═C bond of the molecule. The calculated interface state is located 0.2 eV above the Fermi energy, in agreement with low temperature scanning tunneling spectroscopy local density of states data (0.35 eV), and is responsible for the contrast observed in low bias empty-state STM images.

DOI: 10.1103/PhysRevLett.101.096801 PACS numbers: 73.63.Rt, 07.79.Cz, 37.25.+k, 68.37.Ef

The development of STM has revolutionized the study of surfaces and largely enabled recent developments in nanoscience and technology. STM and its sibling scanning probe methods (SPM) involve local proximal measurements of properties such as density of states or physical and chemical forces. In this mode STM and SPM visualize the surface via the contrast due to local variations in these measurement parameters. Direct interaction between the probe and the surface has also been exploited to manipulate and influence the ordering of atoms and molecules on surfaces [1–4] or to induce local chemical reactions [5–8]. In the visualization mode, while the composition and atomic structure of the probe were recognized as being important in determining the detailed contrast [9,10], the contrast itself was considered to reflect intrinsic properties of the separate probe and surface systems. Only in the case of the enhanced corrugation levels observed on close-packed metal surfaces was there considered to be an explicit interaction between the probe and the surface [11,12]. In that case the contrast was modeled as being due to bond making and breaking events during scanning, which resulted in the probe plucking the atoms on the surface.

Here in this Letter, we demonstrate that specific interactions between the probe and surface may be commonplace particularly in molecular systems where the large HOMO-LUMO gap results in small probe-molecule separations under low bias, high current conditions. We show that in the case of 1,3-cyclohexadiene (1,3-CHD) on Si(100) this probe-molecule interaction creates a specific interface state that is itself directly responsible for the observed image. In contrast to metal systems where the interaction increases the apparent corrugation, here a new state is created close to the Fermi energy (E_f) that dominates transport into the molecule-surface system. These data demonstrate that wide band-gap low-conductance molecules such as 1,3-CHD may form electrically active interface states with metals and that STM can be used to explore contact formation and to screen molecules for potential electronic applications.

Previously, we showed that STM can distinguish between the reaction products of 1,3-CHD on Si(100) [13,14] and directly measures the force of the probe-molecule interaction [15], including the onset of local density of states (LDOS) feature that was attributed to incipient chemical bond formation [16]. Figures 1(a)–1(e) show empty-state STM images of the five different 1,3-CHD attachment geometries in which the single remaining C═C bond appears to be the origin of the contrast

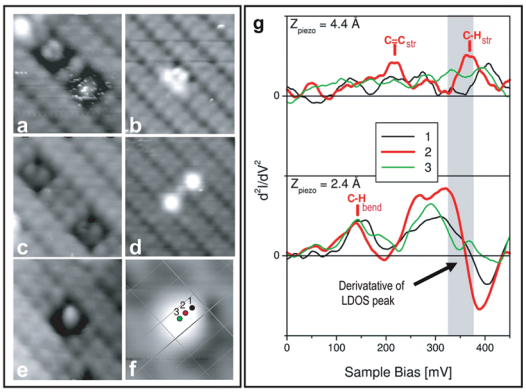

FIG. 1 (color). (a)–(e) are empty-state STM images of the five different 1,3-CHD attachment geometries $V_{\text{sample}} = 1.3$ V. (f) is a close-up of product (c) in which STS spectra (g) are recorded at positions 1–3 at two different heights. Peaks and inflection features (shaded area) in $\frac{d^2I}{dV^2}$ correspond to vibrational modes and LDOS peaks, respectively. Vibrational mode assignment in (g) is based on published IR and HREELS data [31–33]. The spectra in (g) demonstrate the localization of the new interface state to the probe position that corresponds to the center of the remaining C═C bond [position 2 in (f)].

[13,14]. Similar nodal features have also been reported in empty-state images of 1,4-cyclohexadiene adsorbed on the Si(100) surface at a sample bias of +1.3 V [17]. The superior resolution in Fig. 1 was not achieved with all probes, indicating that probe composition and structure is important. Moreover, the double-bond feature is only observed in empty-state imaging conditions and with improved contrast as the sample bias is reduced to +1 V and below [13,14].

On initial inspection, one might attribute the empty-state features in Fig. 1 to the π^* state of the remaining C═C bond in the attached molecule. However, the ability of STM to image the π^* of 1,3-CHD adduct cannot be explained exclusively in terms of the electronic structure of the surface bound molecule. For example, NEXAFS studies of acetylene adsorbed on Si(100) (which also has a single C═C bond remaining after attachment) indicate that the energy of the π and π^* levels associated with the double bond are located approximately −2 and +3 eV with respect to E_f [18]. This result is consistent with our own geometry optimized density-functional theory (DFT) calculations for the 1,3 CHD molecule attached to the Si(100) surface which indicate that for the intradimer product [Fig. 1(a)] the π and π^* levels of the remaining C═C in the molecule are located at −1.6 and +3.5 eV (see Fig. 4). Given that NEXAFS involves the creation of a core hole and hence probes the levels of an effective $Z + 1$ system, and DFT traditionally underestimates the energies of empty states, these data indicate a π^* level located well outside our STM tunneling window. Even allowing for broadening of the π^* state due to hybridization with the bulk Si or local enhancements in the polarizability due to the presence of the molecule, it is not possible to explain the STM and scanning tunneling spectroscopy (STS) results detailed above.

To resolve this discrepancy a series of 13 DFT geometry optimized calculations were performed that included the molecule-surface system and a platinum STM probe (original STM experiments were performed using cleaned W and W probes inked with Pt metal [15,16]). Our calculations were performed using the Cambridge Serial Total Energy Package (CASTEP)[19]. Plane wave (cutoff energy 240 eV) and the PW-91 GGA [20] methods were used with a ($1 \times 3 \times 2$) Monkhorst-Pack grid [21]. Optimizations were carried out using the BFGS scheme [22] where the energy and maximum force convergences were set to 2×10^{-5} eV/atom and 0.05 eV/Å, respectively. Electronic redistribution as a result of the probe-molecule interaction was examined via LDOS, partial (ion and n, l-quantum number decomposed) density of states (PDOS) together with a Mulliken analysis [23] for each of the 13 optimized structures. The PDOS and Mulliken analysis is calculated using projection of the plane wave states onto a localized basis using a technique described by Sanchez-Portal *et al.* [24] and implemented in the CASTEP program.

In our calculations the surface was modeled [see Fig. 3(a)] in a supercell lattice (35.8 Å × 7.68 Å × 11.52 Å) as a six layer deep Si slab with H atoms used to saturate the bottom side of the slab and a vacuum separation of approximately 20 Å. The slab contains three Si-Si surface dimers and the 1,3 CHD molecule is attached to the central dimer in the (4 + 2) intradimer orientation. The STM probe is modeled as a pyramidal cluster of four Pt atoms with interatomic distances and angles taken from the geometry optimized unit cell of the bulk metal. Prior to the introduction of the Pt STM probe the geometry optimized surface-molecule system was generated with a preliminary calculation where the top four layers of the Si slab and the adsorbed molecule were allowed to relax while the bottom two Si layers and H atoms were constrained at bulk positions. The STM probe was then introduced into the supercell with its apex positioned over the center of the C═C bond. Geometry optimizations of the 1,3 CHD molecule on a constrained Si surface, interacting with a constrained probe were then performed at a range of probe to C═C bond separations. The calculations were repeated using a W probe and the computational results are similar to those described herein.

Figure 2(a) shows the interaction energy of the combined system as the probe approaches the molecule. A well-defined binding interaction is observed at a separation of approximately 0.2 nm. We recognize here that the calculated binding interaction (~2 eV) is larger than that typically found for a C═C on a Pt surface [25]. This results from the reduced coordination of the Pt atoms in our model probe. Similar results have been reported for ethene adsorption on Pt where the interaction strength decreases

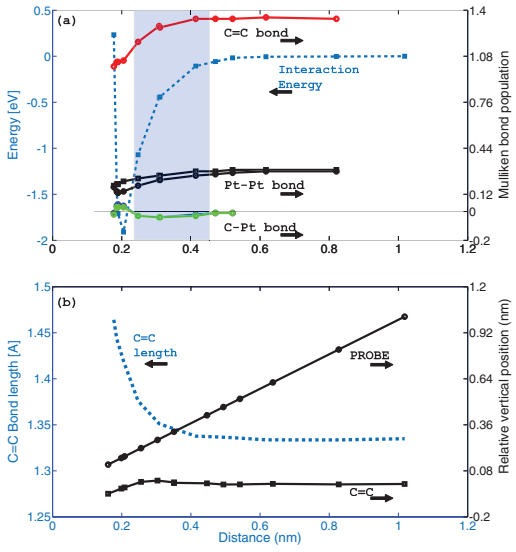

FIG. 2 (color). (a) Interaction potential (left y axis) and Mulliken analysis (right y axis) as a function of the probe to C═C distance, (b) C═C bond length as a function of the probe to C═C distance, and (right y axis) C═C bond height relative to probe position.

with size of the Pt cluster: 1.06 eV with a 7 atom Pt cluster [26], 0.73 eV with a 19 atom Pt cluster [27], to ~0.6 eV using a infinite Pt slab in a periodic calculation [25]. Our attempts to model the interaction using significantly larger probe clusters proved intractable since they also necessitated an extended Si slab. These calculations demonstrate that although the strength of the interaction depends on the size of the probe cluster, the wave functions involved in the binding are not affected.

Also plotted in Fig. 2(a) are the results of the Mulliken analysis for our system. The relative values of Mulliken populations provide a qualitative description of the bonding character between the specified ions [28]. The curves indicate that the strength of the C═C and Pt-Pt bonds weaken as the probe advances from 0.5 nm. Interestingly, this is accompanied (in the 0.45 nm → 0.24 nm *shaded area*) by an antibonding interaction between the frontier Pt and C ions. This antibonding interaction is eventually replaced by bonding character once the interaction distance decreases beyond 0.24 nm. Therefore, while charge transfer is occurring from the probe to the C═C for interaction distances below 0.5 nm the interaction is not fully accompanied by an increase in the bonding character between the Pt and C ions. The specifics of this behavior are expanded upon below.

Figure 2(b) displays the approach trajectory of the probe and the corresponding relaxation of the C═C bond. The C═C is observed to be initially pulled towards the probe and is ultimately compressed toward the surface by the advancing probe, in excellent agreement with the relaxation spectroscopy data [15]. The dashed curve of Fig. 2(b) shows that the C═C bond length increases during the probe trajectory, in agreement with the C═C Mulliken analysis in Fig. 2(a) and the formation of the Pt-C bond. This analysis is consistent with the STS data of Fig. 1(g) recorded at positions 1–3 in Fig. 1(f) and at two different probe separations. At large separations the C-H and C═C stretches are detected locally over the position of the C═C bond but are replaced at smaller separations by a large LDOS feature at 0.35 eV due to bond formation.

The LDOS in four neighboring empty-state energy windows is shown in Fig. 3 as a function of the probe-molecule separation. At large separations, the dominant charge density occurs in the 3–4 eV energy window and represents the π^* level of the molecular adduct, which is weakly mixed with the conduction band levels of the substrate resulting in leakage of charge density to lower (and higher) energies. There is virtually no charge density in the 0–1 eV energy window at large separations, but as the probe approaches there is a continuous increase in the density in this energy window. This charge density results from an interaction between the probe and the C═C bond of the molecule and under empty-state low bias conditions the STM image contrast is dominated by this new state. Note that the charge density distribution closely mimics that of the π^* level, consistent with the STM data in Fig. 1.

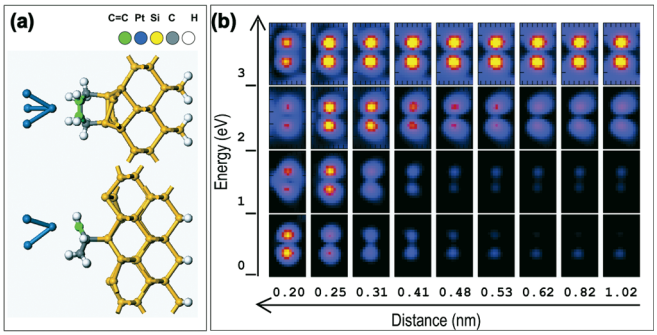

FIG. 3 (color). (a) Schematic of probe-molecule-surface system used in DFT geometry optimization calculations. (b) Tracking the LDOS for a slice positioned 1 Å above the C═C bond as a function of probe position. Charge density from the 3–4 eV energy window is pushed to lower energy as the probe approaches the molecule.

To gain a better understanding of the orbital interactions responsible for this new state, Fig. 4(a) tracks the PDOS for a C $2p$ state centered on one of the atoms of the C═C bond as a function of the probe-molecule separation. At large separations the energy of the π and π^* states are localized at -1.5 and $+3.5$ eV, respectively. As the probe-molecule distance decreases each state becomes broadened and is accompanied by the growth of a new state with p character $+0.2$ eV above E_f. This behavior, together with the Mulliken analysis of Fig. 2(a), can be rationalized by appealing to the bonding in a closely related system: the Chatt-Dewar-Duncanson model [29] for transitional metal η^2-alkene complexes. Figure 4(b) shows a molecular orbital correlation diagram in which the olefin donates charge

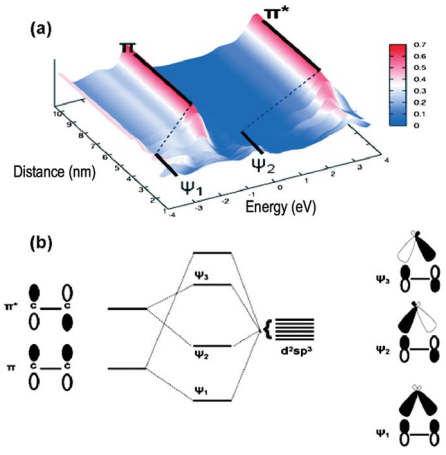

FIG. 4 (color). (a) PDOS for a C $2p$ state centered on one of the atoms of the C═C bond as a function of probe-molecule separation. Localization of the π and π^* states is seen to decrease and is accompanied by the growth of a state with C $2p$ character 0.2 eV above E_f. (b) A conceptual molecular orbital diagram appropriate for η^2-alkene complexes. Competition between the Ψ states can account for the Mulliken analysis of the Pt-C bond of Fig. 2(a).

into empty metal orbitals (to form Ψ_1), and is accompanied by back donation from filled metal orbitals into the empty olefin orbital (to form Ψ_2 and Ψ_3). The PDOS peaks in Fig. 4(a) have been labeled with the aid of the correlation diagram in Fig. 4(b) and the excellent agreement demonstrates that the interaction between the probe and the molecules is well described by Fig. 4(b). In particular the Ψ_2 level at +0.2 eV agrees well with the +0.35 eV feature in the LDOS reported previously at small probe-molecule separations [16].

Within this framework, the Ψ_2 and Ψ_3 interaction serve to donate charge into the π^* of the C═C bond, whereas Ψ_2 and Ψ_1 interaction lead to the formation of the Pt-C bond. At large probe separations [shaded area in Fig. 3(a)] charge transfer to the C═C dominates and results in the weakening of the Pt-Pt and C═C bonds, in agreement with the Mulliken analysis in Fig. 3(a). This Pt-C═C backbonding interaction is energy lowering due to charge delocalization. Eventually for reduced probe separation the bonding contribution of Ψ_2 aided by Ψ_1 prevails resulting in the establishment of the Pt-C bond, and the interface state observed by STM.

Collectively, the results in Figs. 2–4 demonstrate that during typical STM operation the probe may strongly interact with molecular systems, particularly those with large intrinsic HOMO-LUMO gaps. In instances where this interaction produces an interface state that is within the tunneling energy a new conductance channel and hence a new image contrast mechanism emerges. Conversely, controlled STM studies provide a means to explore how the intrinsic properties of molecules are affected by contact formation, with potential applications in the area of molecular devices. The controlled formation of interface states opens up significant opportunities in the development of negative differential resistance (NDR) behavior in molecular electronic devices [30]. Large NDR effects are predicted in metal-molecule-metal systems with localized filled and empty interfaces states either side of the molecule. The results presented here conclusively demonstrate that STM is particularly sensitive to the development of electrically active interface states (close to E_f) and hence provides a straightforward method to identify interesting metal-molecule combinations for potential NDR device applications.

This work was supported by Science Foundation Ireland under Grant No. 06/IN.1/I106. We would also like to thank Professor Graeme Watson and the Trinity Center for High Performance Computing for assistance.

*Present address: Savannah River National Laboratory, Aiken, SC, USA.

[1] A. J. Heinrich, C. P. Lutz, J. A. Gupta, and D. M. Eigler, Science **298**, 1381 (2002).
[2] H. C. Manoharan, C. P. Lutz, and D. M. Eigler, Nature (London) **403**, 512 (2000).
[3] T. W. Fishlock and A. Oral, Nature (London) **404**, 743 (2000).
[4] G. Meyer *et al.*, Phys. Rev. Lett. **78**, 1512 (1997).
[5] S.-W. Hla, G. Meyer, and K.-H. Rieder, Chem. Phys. Lett. **370**, 431 (2003).
[6] K. Morgenstern and K.-H. Rieder, Chem. Phys. Lett. **358**, 250 (2002).
[7] B. C. Stipe *et al.*, Phys. Rev. Lett. **78**, 4410 (1997).
[8] J. R. Hahn and W. Ho, Phys. Rev. Lett. **87**, 166102 (2001).
[9] W. A. Hofer, A. J. Fisher, G. P. Lopinski, and R. A. Wolkow, Phys. Rev. B **63**, 085314 (2001).
[10] W. A. Hofer, J. Redinger, and R. Podloucky, Phys. Rev. B **64**, 125108 (2001).
[11] A. R. H. Clarke *et al.*, Phys. Rev. Lett. **76**, 1276 (1996).
[12] W. A. Hofer, A. Garcia-Lekue, and H. Brune, Chem. Phys. Lett. **397**, 354 (2004).
[13] L. C. Teague and J. J. Boland, J. Phys. Chem. B **107**, 3820 (2003).
[14] L. C. Teague, D. Chen, and J. J. Boland, J. Phys. Chem. B **108**, 7827 (2004).
[15] B. Naydenov, P. Ryan, L. C. Teague, and J. J. Boland, Phys. Rev. Lett. **97**, 098304 (2006).
[16] B. Naydenov, L. C. Teague, P. Ryan, and J. J. Boland, Nano Lett. **6**, 1752 (2006).
[17] K. Hamaguchi *et al.*, J. Phys. Chem. B **105**, 3718 (2001).
[18] F. Matsui, H. W. Yeom, I. Matsuda, and T. Ohta, Phys. Rev. B **62**, 5036 (2000).
[19] M. D. Segall *et al.*, J. Phys. Condens. Matter **14**, 2717 (2002).
[20] J. P. Perdew *et al.*, Phys. Rev. B **46**, 6671 (1992).
[21] H. J. Monkhorst and J. D. Pack, Phys. Rev. B **13**, 5188 (1976).
[22] T. H. Fischer and J. Almlof, J. Phys. Chem. **96**, 9768 (1992).
[23] R. S. Mulliken, J. Chem. Phys. **23**, 1833 (1955).
[24] D. Sanchez-Portal, E. Artacho, and J. M. Soler, Solid State Commun. **95**, 685 (1995).
[25] G. W. Watson, R. P. K. Wells, D. J. Willock, and G. J. Hutchings, J. Phys. Chem. B **104**, 6439 (2000).
[26] R. M. Watwe, B. E. Spiewak, R. D. Cortright, and J. A. Dumesic, J. Catal. **180**, 184 (1998).
[27] J. Shen *et al.*, J. Phys. Chem. B **103**, 3923 (1999).
[28] M. D. Segall, R. Shah, C. J. Pickard, and M. C. Payne, Phys. Rev. B **54**, 16 317 (1996).
[29] J. Chatt and L. A. Duncanson, J. Chem. Soc. 2939 (1953).
[30] H. Dalgleish and G. Kirczenow, Phys. Rev. B **73**, 245431 (2006).
[31] B. Naydenov and W. Widdra, J. Chem. Phys. **127**, 154711 (2007).
[32] M. J. Kong *et al.*, J. Phys. Chem. B **104**, 3000 (2000).
[33] H. S. Kato, M. Wakatsuchi, M. Kawai, and J. Yoshinobu, J. Phys. Chem. C **111**, 2557 (2007).